ADVANCED FUNCTIONAL MATERIALS
www.afm-journal.de

Polarization-Multiplexed Silicon Metasurfaces for Multi-Channel Visible Light Modulation

Wei Zhu, Yuancheng Fan, Ruisheng Yang, Guangzhou Geng, Quanhong Fu, Changzhi Gu, Junjie Li,* and Fuli Zhang**

All-dielectric metasurfaces with low-loss planar photonic subwavelength elements can be freely designed to realize high-efficiency light wave manipulation. It is highly desirable to achieve multifunctionalities with a single metasurface to further enrich the manipulation of light with metasurfaces for diverse applications. This article demonstrates multifunctional silicon-based metasurfaces capable of generating versatile wavefronts under different polarization light incidence at visible wavelengths. The polarization-multiplexed metasurfaces are implemented with rationally arranged anisotropic silicon nanobricks to achieve independent control of orthogonal linearly polarized light waves for multi-channel functionalities, including polarized beam splitting, opposite charged and different ordered optical vortexes. The polarization-multiplexed high-quality silicon metasurfaces have great potential for applications in multi-channel optical devices with integrated functionality.

1. Introduction

Optical metasurfaces[1–4] composed of artificially structured planar subwavelength nanostructures have inspired increasing significant research works due to their extraordinary capability for novel manipulation on optical fields. Conventional optical devices are based on the propagation of light in natural materials, which are often bulky and hard to be integrated into modern nanophotonics. In contrast, metasurfaces can manipulate the wavefront of light by designing periodic/aperiodic subwavelength nanostructures with extreme anisotropy. Moreover, the planar characteristics of metasurfaces make them easier to design, integrate multiple functions, and fabricate. Recently, plenty of functional metasurface devices have been reported, including metagratings,[5–8] high quality factor devices,[9,10] spontaneous emission control,[11–13] magnetic mirrors,[14] cloaking,[15–20] optical vortex beam generators,[21–25] and so on.[26–39]

In order to achieve the desired functionality with high efficiency, the materials used to fabricate metasurfaces should not only strongly interact with light but also have low intrinsic losses. Metal-based plasmonic metasurfaces[40–42] and dielectric-based Mie metasurfaces[43–45] are the predominantly two class strategies for enhancing the light and matter interactions with resonant subwavelength structures. In the plasmonic metasurfaces, the interaction between the incident photons and the free electrons in the metal is generally accompanied by a mutual transformation of energy and momentum. In the dielectric metasurfaces, the dielectric nanoparticles are designed to further localize light in a subwavelength volume.[46,47] However, the plasmonic metasurfaces show high inherent non-radiative ohmic losses at optical frequencies which inevitably hinder their promising applications.[48,49] For improving the efficiency, reflective metasurfaces[50] and all-dielectric metasurfaces[51] are exploited to decrease the propagation loss. Reflective metasurfaces are limited in the application of optical devices due to the reflection configuration. All-dielectric metasurfaces can avoid the strong absorption losses by an elaborate arrangement of high-index and low-loss dielectric nanostructures.[52,53] Dielectric metasurfaces exploiting the Pancharatnam–Berry phase (PB phase) can achieve full range (2π) phase control by rotating the orientation angle of high aspect ratio anisotropic nanostructures with identical geometry.[53,54] There are many transmissive dielectric metasurfaces based on the PB phase[55–57] that have been reported, but these metasurfaces are limited for manipulating circularly polarized light, while seldom works have been reported for the independent manipulation of two orthogonal linearly polarized light.

W. Zhu, Y. Fan, R. Yang, Q. Fu, C. Gu, F. Zhang
Key Laboratory of Light Field Manipulation and Information Acquisition
Ministry of Industry and School of Physical Science and Technology
Northwestern Polytechnical University
Xi'an 710129, China
E-mail: phyfan@nwpu.edu.cn; fuli.zhang@nwpu.edu.cn

W. Zhu, G. Geng, J. Li
Beijing National Laboratory for Condensed Matter physics
Institute of Physics
Chinese Academy of Sciences
Beijing 100190, China
E-mail: jjli@iphy.ac.cn

R. Yang
Department of Electrical and Computer Engineering
National University of Singapore
Singapore 117583, Singapore

J. Li
School of Physical Sciences
CAS Key Laboratory of Vacuum Physics
University of Chinese Academy of Sciences
Beijing 100049, China

J. Li
Songshan Lake Materials Laboratory
Dongguan, Guangdong 523808, China

The ORCID identification number(s) for the author(s) of this article can be found under https://doi.org/10.1002/adfm.202200013.

DOI: 10.1002/adfm.202200013

Here, we show a multiplexed metasurface platform that provides polarization-dependent functionality based on an elaborate arrangement of silicon rectangular nanobricks with high transmission efficiency. Compared with other proposed multifunctional metasurface,[58–61] the polarization-multiplexed metasurface we proposed enable to realize independent manipulation of orthogonal linearly polarized light beams in: i) polarization-dependent beam deflectors that can refract *x*-linear polarized (XLP) and *y*-linear polarized (YLP) incident lights into opposite directions with designed angles; ii) vortex beam generators that convert Gaussian beams into opposite charged and different ordered orbital angular momentum (OAM) light beams. Such multi-channel polarization-multiplexed metadevices enable the realization of unique extensibility and flexibility in versatile photonic devices, which may provide an increasing possibility for next-generation ultrahigh-speed and high-capacity optical communications.

2. Results and Discussion

The schematic of the metasurface platform is shown in **Figure 1**a, which is composed of a single-layer high refractive index polysilicon nanobricks standing on a fused silica substrate. The pitches of the nanobrick array along the *x* and *y* directions are identical and denoted as *P*. The height of the silicon nanobrick *h* is 340 nm on the 500 μm thick fused silica. And the length of nanobrick along the *x* and *y* directions are P_x and P_y. For achieving the polarization-dependent response of the metasurface, we assume that the electric field component of the incident linearly plane wave normally is along the *x*- or *y*-axis. In this way, the cross-polarization electromagnetic waves can be ignored because of their low transmittance. However, it will not hinder the accumulation of different phases for co-polarized electromagnetic waves along the *x* and *y* directions, respectively.

We employed a finite difference time domain (FDTD)-based electromagnetic solver to perform numerical simulation of the metasurfaces, the incident electromagnetic field is set as a plane wave propagating along negative *z*-axis with electric and magnetic fields along *y*- and *x*-axes, respectively. The refractive index and extinction coefficient of polysilicon from 400 to 940 nm are measured by ellipsometer after being deposited by ICP-CVD, as shown in Figure 1b. In our calculations, the refractive index of the polysilicon is 3.686–0.028i at a wavelength of 633 nm. And the refractive index of the fused silica is 1.46. For the given pitch of 270 nm, we first calculated transmission efficiencies as the functions of the nanobrick dimensions along the *x*- and *y*-axis, P_x and P_y, with the range from 50 to 180 nm, under the XLP and YLP incidences, respectively. For the convenience of subsequent design, the diameter and transmission efficiencies were recovered as a function of the phase shift by minimizing the following equation.

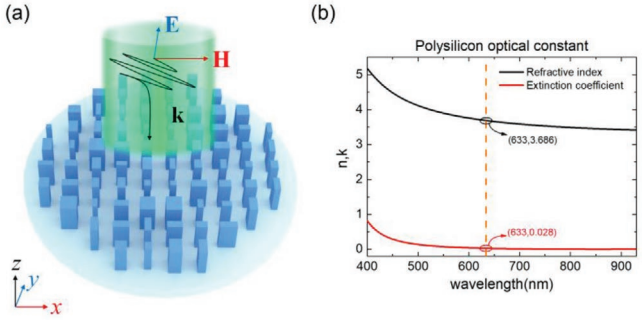

Figure 1. a) Schematic diagram of the polysilicon nanobrick arrays on the fused silica with refractive index of $n = 1.46$. The length and width of the nanobrick along the *x*-axis and *y*-axis are P_x and P_y, which are varied by the difference phases of transmission. The interval of the adjacent unit cell is $p = 270$ nm, and the height of the nanobricks are $h = 340$ nm. b) The measured optical constants of polysilicon which are deposited by ICP-CVD.

$$\mathrm{MSE} = \frac{1}{2}\left[\left|t_x - \exp\left(i\phi_x\right)\right|^2 + \left|t_y - \exp\left(i\phi_y\right)\right|^2\right] \quad (1)$$

where t_x/t_y and φ_x/φ_y are the complex transmittance and the abrupt phase shifts imparted by the two arms of the nanobrick with XLP and YLP incident light.[62] According to Equation (1), we can obtain the maximum transmittance by minimizing the value of mean square error (MSE). Before obtaining the proper appropriate geometric size of the nanobricks, we are supposed to confirm that the size range of the nanobricks from 50 to 180 nm has covered the 0 to 2π variation of the phase. In this way, we can realize the polarization multiplex by manipulating the wavefront of transmitted XLP and YLP light, respectively.

The metasurface we demonstrated can realize 0 to 2π variation of the phase when the geometric of the size of the nanobricks varied from 50 to 180 nm. The nanobrick can achieve 0 to 2π phase variation by only changing the length of the nanobrick along the *x* direction under the XLP incidence when the other length of nanobrick is fixed in the *y* direction. Analogously, due to the symmetry of the nanobricks, phase control can also be realized along *y* direction under YLP incidence. Note that the possibility of varying the dimensions of the nanoblocks in both *x* and *y* directions will add additional degrees of freedom in both directions. Therefore, the method of reversal extracting the structure size by phase distribution is adopted, and recovered results are shown in **Figure 2**, every phase from –180° to 180° has the corresponding geometric size of the nanobrick whether in *x* or *y* directions. And it is convenient to figure out the transmittance with the different phases. So, according to the relationship between φ_x/φ_y and P_x/P_y shown in Figure 2a,b, we are able to accurately find the appropriate geometry with the phase shift while ensuring the high transmittance of the metasurface. Figure 2c,d, has shown the transmittance when φ_x and φ_y are fixed, which are corresponding to Figure 2a,b.

For simplifying the process of the design, the non-uniform array is typically approximated by the uniform periodic array. But the approximate condition is that light must be well confined in the nanobricks and the coupling between adjacent nanostructures is weak, which enables independent modulation of phases along the *x*-axis and *y*-axis with a single unit cell. As shown in **Figure 3**, the uniform array of nanobricks with a geometric size of $P_x = P_y = 127$ nm was used to verify the approximation of the local effect. It is clearly shown that the H field is strongly confined in the nanobrick which is surrounded

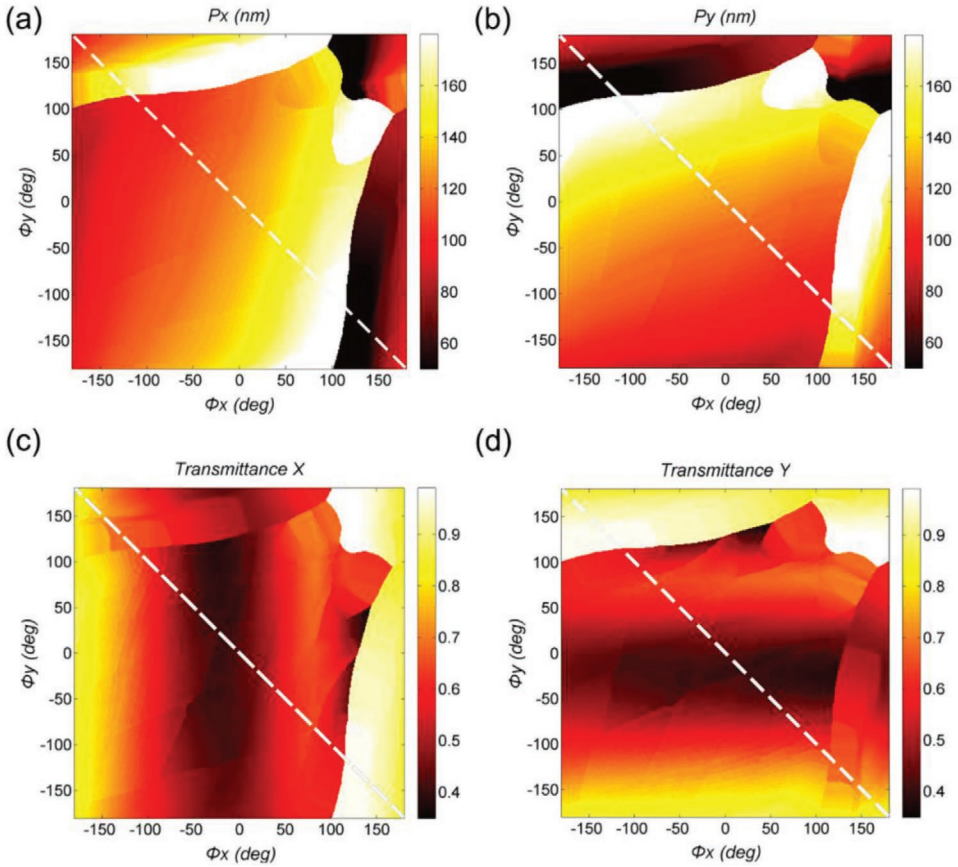

Figure 2. Simulated result of a) P_x, b) P_y and transmittance c) $|t_x|^2$, d) $|t_y|^2$ as functions of varied phase for *x* and *y* polarized incident light.

by white dash lines, which shows the coupling between the nanobricks is weak. At the same time, weak coupling among nanobricks makes the approximation valid.

In order to realize complete manipulation of the wavefront, we choose eight discrete nanobricks with $\pi/4$ changes to cover the 0–2π phase by seeking the appropriate P_x and P_y along the reverse diagonal in Figure 2a,b. For the realization of the separate manipulation of XLP and YLP incident light, adjacent nanobricks have opposite phase changes in different polarizations. **Table 1** shows transmitted light phase variation from –180° to 180° and transmittance depending on optimized nanobricks dimensions.

In order to verify the performance of the metasurface, we experimentally demonstrated high-efficiency full-phase manipulation with the multi-channel metasurface at visible wavelength enabling two practical functionalities: optical beam deflector and vortex beam generator.

The optical beam deflector consists of the periodically arranged supercells which contain eight nanobricks from Table 1, whose radius is increased from 80 to 180 nm in steps

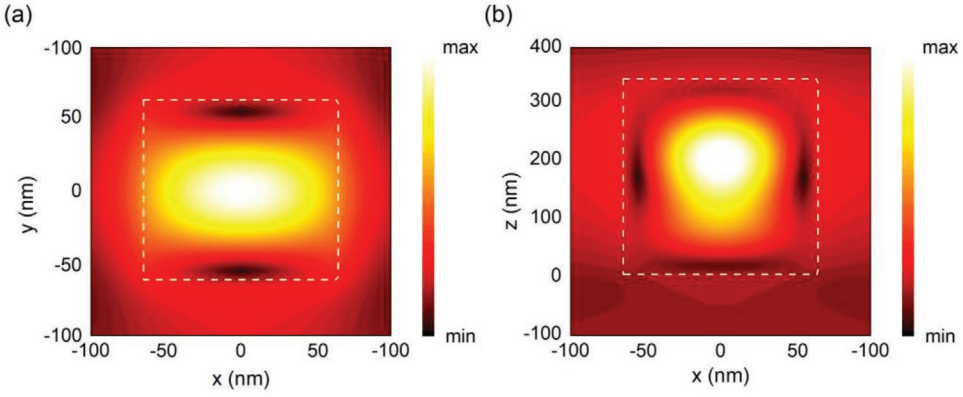

Figure 3. The distribution of the H field in the polysilicon nanobrick at cross-section of a) *xoy* plane and b) *xoz* plane, respectively.

Table 1. Parameter setting and the transmission properties for the optimized nanobricks.

Nanobrick	1	2	3	4	5	6	7	8
T_x [/t_x/2]	0.81	0.65	0.59	0.4	0.44	0.55	0.62	0.97
T_y [/t_y/2]	0.84	0.97	0.62	0.55	0.44	0.4	0.59	0.65
Φ_x [deg]	–180	–135	90	–45	0	45	90	135
Φ_y [deg]	180	135	90	45	0	–45	–90	–135
P_x [nm]	97	152	100	112	127	148	175	50
P_y [nm]	97	50	175	148	127	112	100	152

of 1 nm. In the x/y direction, adjacent nanobricks have phase shifts with π/4 increments/decrements. Certainly, the number of nanobricks in supercell can change as long as it covers the 2π phase. Therefore, polarization-dependent optical beam deflectors are able to realize by reverse extracting the phase with an arbitrarily fixed difference. In this way, a polarization-multiplexed beam deflector that can manipulate XLP and YLP light separately has been designed.

The refraction angle of incident light can be calculated by the generalized Snell's law: $n_t \sin(\theta_t) - n_i \sin\theta_i = \frac{\lambda_0}{2\pi}\frac{d\varphi}{dx}$,[63] where the θ_t and θ_i are the refracted angle and incident angle of transmitted light, respectively, n_t and n_i are the refractive indexes of the media in the both sides of the interface, respectively, λ_0 is the wavelength of light in vacuum and $d\phi/dx = 2\pi/L$ is the phase gradient. **Figure 4**a,e shows two metasurfaces that can deflect optical beams with a difference angle by changing the geometric size of nanobricks. Figure 4b,f shows scanning electron microscopy (SEM) images for a fabricated polarization-dependent beam deflecting metasurface with 324 × 324 μm total size. As shown in the top panel of Figure 4a, the supercell A can realize the 2π phase transition whether in the x or y direction. The simulated results in Figure 4c show the normal incidence of a light beam will be deflected by 17° when the period of the supercell L = 2.16 μm. Compared to supercell A, supercell B realizes 4π phase transition in y direction while 2π phase transition in the x direction. So, metasurface which consists of supercell B is able to deflect XLP and YLP lights with difference angles, as shown in Figure 4g. In y direction, the angle of deflection is 34° due to supercell B can realize the full-phase manipulation at the length of L/2.

Note that the angles of the deflection can be arbitrarily controlled by changing the periodical length L of the supercell. The periodical length of the supercell is expressed as $L = p \times N$, where p is the length of the unit cell, and N is the number of nanobricks in one supercell. Since the length of the unit cell is fixed, the way we modulate the desired refracted angles is by adjusting the number of the used nanobricks N. With the decrement of the periodical length L of the supercell, the angle of the deflection will increase. To ensure the correction of the phase distribution, the relation between the nanobrick dimensions and phases should be recalculated and reselected. Compared to the angle of deflection of XLP and YLP incident light in Figure 4g, it is clear that the coupling effect between adjacent nanobricks has been enhanced with decreasing of the length L. So, the designed metasurface can manipulate the XLP and YLP lights to the arbitrary angle of deflection with high transmission efficiency. In the experiment, camera images of input and output beams with measured transmission power to desired order normalized on input power to be around 54.7%/58.6% and 57.3%/46.9% for XLP and YLP 633 nm laser incident light as shown in Figure 4d,h. Interestingly, whatever simulated normalized transmitted curve or experimental date show, the transmittance will decrease with the increase of the deflected angle. The efficiency of the beam deflector is determined by the average transmittance of all the unit cells in the supercell, since the beam deflector is composed of periodic supercells. In this way, it is clearly shown that the relatively high efficiency of the beam deflector could be realized as long as the transmittance of each unit cell that composes the supercell is guaranteed, while the efficiency of deflected beam inevitably decreases with the increase of the deflected angle.[64]

To further demonstrate the flexibility of designed polarization-multiplexed silicon metasurface, we have fabricated a vortex converter that is able to convert a Gaussian beam into a vortex beam possessed helical wavefront with arbitrary topological charges by appropriate arrangement of nanobricks. In addition, the vortex converter we designed can realize OAM beams with different topological charge by controlling the polarization of incident light. There is no doubt that the function will greatly increase the capacity of the communication channel.

Schematics of our designed vortex converter (l_x = 1, l_y = –1) is shown in the top panel of **Figure 5**a, the plane is divided into eight sectors that have contained 2π phase shift. The sign of the topological charge represents the direction of the vortex. And it is clear that adjacent sectors have π/4 phase increment/decrement in XLP/YLP light from the first quadrant to the fourth quadrant along the counter-clockwise. In this way, transmitted lights will obtain the opposite OAM after XLP and YLP pass through the metasurface, as shown in Figure 5c. Simultaneously, we have also considered the circumstance that polarization-multiplexed OAM beams, as shown in Figure 5d. Furthermore, the polarization-multiplexed metasurface design can realize the l_x = 1 and l_y = –2 by arranging the optimized dimension of the nanobricks regularly when the polarization lights with different directions incidence. We fabricate the size of the vortex converter with 324 μm × 324 μm for the convenience of the experiment, and its SEM image is shown in Figure 5b,e. We performed numerical simulations for a reduced size model with 10 μm × 10 μm size to reduce calculation time and memory consumption. Metasurface with reconstructed phase as in Figure 5d can realize the different modulated effects for YLP and XLP light. Compared to the XLP light, it can not only obtain the continuous vortex phase but there will be two singularities appearing in the middle of the beam. As shown in the experimentally measured interferogram in Figure 5j,i, it is clearly proved that the vortex converter we fabricated can transform the linear beams to vortex beams

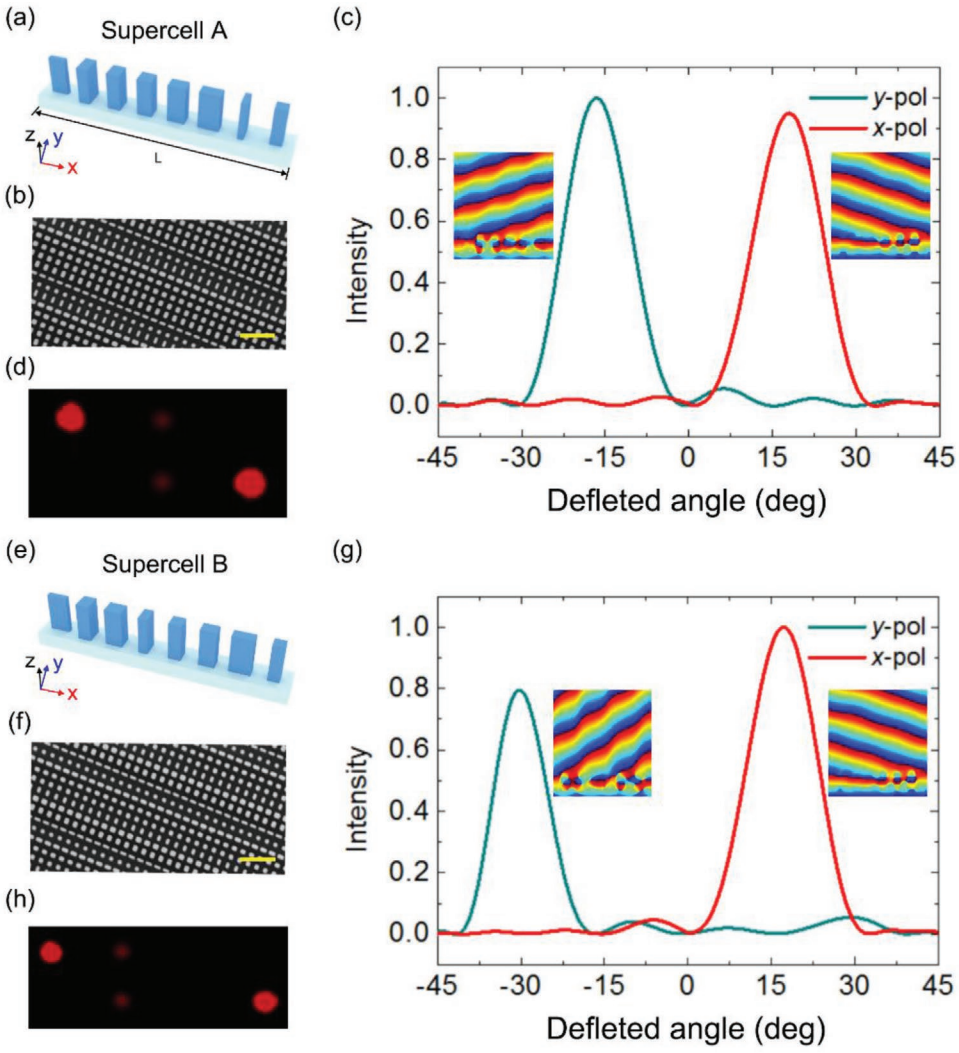

Figure 4. a,e) Schematics of the proposed two beam deflector containing eight nanoblocks, which can realize the full 2π phase shift. b,f) Scanning electron microscopy image of fabricated metasurfaces with 324×324 μm total size. (yellow scale bar: 1 μm) c,g) Difference deflected angle of XLP and YLP incident light with metasurface A and metasurface B (inset: numerically simulated phase of plane wave propagate through the different metasurfaces.) d,h) Beam position with metasurface A and metasurface B; the beam power is refracted to the left side and right side with same distance and different distance due to the phase control derive from the different display of the unit cell.

due to the appearance of interference fringes. In addition, the amounts of characteristic fork features in Figure 5j differ from Figure 5i, which proves the topological charges of transmitted light are polarization dependent. It is worth emphasizing here that the second-order interference fringe has transferred to two first-order interference fringes due to the split of the light with high-order topological charges during transmission. The transmitted power normalized to input power is measured to be 48.3% by a power meter, which is lower than the numerically simulated value due to the absorption of substrate and the deviation of fabricated samples.

3. Conclusion

In summary, we have experimentally demonstrated a multiplexed metasurface platform capable of generating versatile wavefronts depending on the polarization of light incidence at visible wavelengths. The metasurface platform enables arbitrarily manipulation of the XLP and YLP incident light by exactly optimizing the long and short axis of the silicon nanobricks and 2D plane arrangement order. For verifying the functions of our metadevices, we have designed and fabricated a polarization-dependent beam deflector that deflects the XLP and YLP light to different angles with high transmittance of 58.6%/46.9%, and vortex generator that assigns different topological charges to XLP and YLP incident light with high transmittance of 56.3%/48.3%. We can not only control the refraction angles but also the topological charges of the light at will by exploiting the efficient low-loss silicon metasurface platform. Considering the high-efficiency and multi-channel characteristics of the metasurface designs, it is promising for integrated nanophotonics-based applications such as high-capacity optical communications and information encryption.

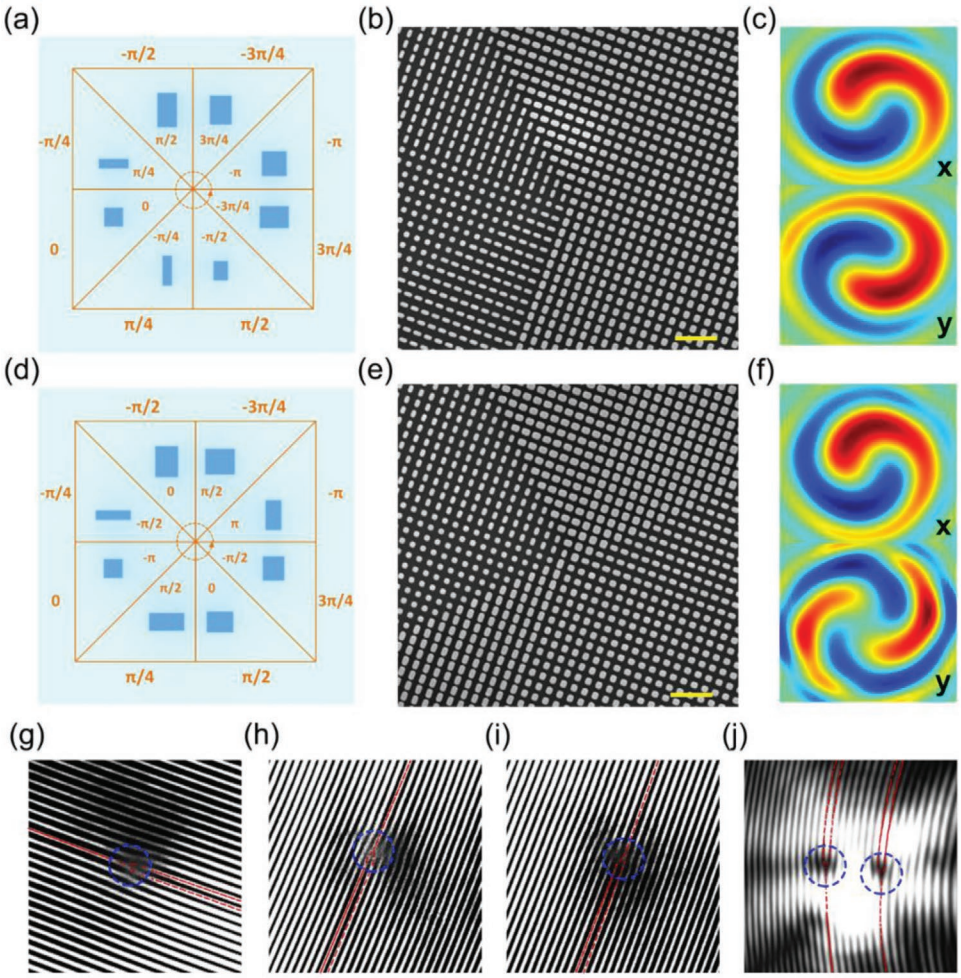

Figure 5. a,d) Schematics of the proposed two metasurfaces which can transform the linearly beam into a beam with OAM. b,e) Scanning electron microscopy image of fabricated metasurfaces with 324 μm × 324 μm total size. c,f) Numerically simulated the distribution of the electric field component of plane wave due to the different arrangement of the nanobricks of the metasurfaces. g–j) Beams with different OAM and Gaussian beams interference experiment results showing spiral-shaped and fork-like intensity distribution. (yellow scale bar: 1 μm).

Acknowledgements

The authors acknowledge the financial support received from the National Natural Science Foundation of China (Grants Nos. 61771402, 12074314, U21A20140, 12074420, 61888102), Strategic Priority Research Program of the Chinese Academy of Sciences under (Grant No. XDB33000000), Key Research Program of Frontier Sciences-CAS (Grant No. QYZDJ-SSWSLH042), the Shenzhen Science and Technology Innovation Commission (JCYJ20170817162221169), Beijing Municipal Science & Technology Commission, Administrative Commission of Zhongguancun Science Park (No. Z211100004821009), and the China Scholarship Council (202106290086).

Conflict of Interest

The authors declare no conflict of interest.

Data Availability Statement

The data that support the findings of this study are available from the corresponding author upon reasonable request.

Keywords

dielectric metasurfaces, high efficiency, metamaterials, multi-channel, polarization control

Received: January 1, 2022
Revised: February 9, 2022
Published online:

[1] L. Huang, X. Chen, H. Mühlenbernd, H. Zhang, S. Chen, B. Bai, Q. Tan, G. Jin, K.-W. Cheah, C.-W. Qiu, *Nat. Commun.* **2013**, *4*, 2808.
[2] A. V. Kildishev, A. Boltasseva, V. M. Shalaev, *Science* **2013**, *339*, 1232009.
[3] D. Lin, P. Fan, E. Hasman, M. L. Brongersma, *Science* **2014**, *345*, 298.
[4] N. Yu, F. Capasso, *Nat. Mater.* **2014**, *13*, 139.
[5] S. Sun, K.-Y. Yang, C.-M. Wang, T.-K. Juan, W. T. Chen, C. Y. Liao, Q. He, S. Xiao, W.-T. Kung, G.-Y. Guo, *Nano Lett.* **2012**, *12*, 6223.
[6] Y. Ra'di, D. L. Sounas, A. Alu, *Phys. Rev. Lett.* **2017**, *119*, 067404.
[7] A. M. Wong, G. V. Eleftheriades, *Phys. Rev. X* **2018**, *8*, 011036.

[8] N. M. Estakhri, V. Neder, M. W. Knight, A. Polman, A. Alù, *ACS Photonics* **2017**, *4*, 228.
[9] A. Tripathi, H.-R. Kim, P. Tonkaev, S.-J. Lee, S. V. Makarov, S. S. Kruk, M. V. Rybin, H.-G. Park, Y. Kivshar, *Nano Lett.* **2021**, *21*, 6563.
[10] R. Yang, J. Xu, N. H. Shen, F. Zhang, Q. Fu, J. Li, H. Li, Y. Fan, *InfoMat* **2021**, *3*, 577.
[11] I. Staude, V. V. Khardikov, N. T. Fofang, S. Liu, M. Decker, D. N. Neshev, T. S. Luk, I. Brener, Y. S. Kivshar, *ACS Photonics* **2015**, *2*, 172.
[12] Z. Wang, K. Yao, M. Chen, H. Chen, Y. Liu, *Phys. Rev. Lett.* **2016**, *117*, 157401.
[13] Y. Bao, Q. Lin, R. Su, Z.-K. Zhou, J. Song, J. Li, X.-H. Wang, *Sci. Adv.* **2020**, *6*, eaba8761.
[14] S. Liu, M. B. Sinclair, T. S. Mahony, Y. C. Jun, S. Campione, J. Ginn, D. A. Bender, J. R. Wendt, J. F. Ihlefeld, P. G. Clem, *Optica* **2014**, *1*, 250.
[15] W. Cai, U. K. Chettiar, A. V. Kildishev, V. M. Shalaev, *Nat. Photonics* **2007**, *1*, 224.
[16] D. Schurig, J. Mock, B. Justice, S. A. Cummer, J. B. Pendry, A. Starr, D. Smith, *Science* **2006**, *314*, 977.
[17] P. Y. Chen, J. Soric, A. Alù, *Adv. Mater.* **2012**, *24*, OP281.
[18] B. Zheng, Y. Yang, Z. Shao, Q. Yan, N.-H. Shen, L. Shen, H. Wang, E. Li, C. M. Soukoulis, H. Chen, *Research* **2019**, *2019*, 8282641.
[19] Y. Li, C. Liu, P. Li, T. Lu, C. Chen, Z. Guo, Y. Su, L. Qiao, J. Zhou, Y. Bai, *Adv. Funct. Mater.* **2020**, *30*, 2003270.
[20] R. Peng, Z. Xiao, Q. Zhao, F. Zhang, Y. Meng, B. Li, J. Zhou, Y. Fan, P. Zhang, N.-H. Shen, *Phys. Rev. X* **2017**, *7*, 011033.
[21] M. I. Shalaev, J. Sun, A. Tsukernik, A. Pandey, K. Nikolskiy, N. M. Litchinitser, *Nano Lett.* **2015**, *15*, 6261.
[22] M. Q. Mehmood, S. Mei, S. Hussain, K. Huang, S. Y. Siew, L. Zhang, T. Zhang, X. Ling, H. Liu, J. Teng, A. Danner, S. Zhang, C. W. Qiu, *Adv. Mater.* **2016**, *28*, 2533.
[23] G. Ruffato, M. Massari, F. Romanato, *Light: Sci. Appl.* **2019**, *8*, 113.
[24] B. Wang, W. Liu, M. Zhao, J. Wang, Y. Zhang, A. Chen, F. Guan, X. Liu, L. Shi, J. Zi, *Nat. Photonics* **2020**, *14*, 623.
[25] K. Ou, G. Li, T. Li, H. Yang, F. Yu, J. Chen, Z. Zhao, G. Cao, X. Chen, W. Lu, *Nanoscale* **2018**, *10*, 19154.
[26] Y. Wen, J. Zhou, *Research* **2019**, *2019*, 8959285.
[27] T. J. Cui, S. Liu, G. D. Bai, Q. Ma, *Research* **2019**, *2019*, 2584509.
[28] S. Wang, P. C. Wu, V. C. Su, Y. C. Lai, C. H. Chu, J. W. Chen, S. H. Lu, J. Chen, B. Xu, C. H. Kuan, T. Li, S. Zhu, D. P. Tsai, *Nat. Commun.* **2017**, *8*, 187.
[29] H. Lu, B. Zheng, T. Cai, C. Qian, Y. Yang, Z. Wang, H. Chen, *Adv. Opt. Mater.* **2020**, *9*, 2001311.
[30] Q. He, S. Sun, L. Zhou, *Research* **2019**, *2019*, 1849272.
[31] C. Lan, H. Ma, M. Wang, Z. Gao, K. Liu, K. Bi, J. Zhou, X. Xin, *ACS Appl. Mater. Interfaces* **2019**, *11*, 14229.
[32] C. Sheng, H. Liu, H. Chen, S. Zhu, *Nat. Commun.* **2018**, *9*, 4271.
[33] Z.-L. Deng, J. Deng, X. Zhuang, S. Wang, T. Shi, G. P. Wang, Y. Wang, J. Xu, Y. Cao, X. Wang, *Light: Sci. Appl.* **2018**, *7*, 78.
[34] Z. Liu, H. Du, Z.-Y. Li, N. X. Fang, J. Li, *APL Photonics* **2018**, *3*, 100803.
[35] X. Niu, X. Hu, Y. Xu, H. Yang, Q. Gong, *Adv. Photonics Res.* **2021**, *2*, 2000167.
[36] S. Chen, W. Liu, Z. Li, H. Cheng, J. Tian, *Adv. Mater.* **2020**, *32*, 1805912.
[37] F. Zangeneh-Nejad, R. Fleury, *Phys. Rev. Lett.* **2020**, *125*, 054301.
[38] S. Dai, Q. Ma, M. K. Liu, T. Andersen, Z. Fei, M. D. Goldflam, M. Wagner, K. Watanabe, T. Taniguchi, M. Thiemens, F. Keilmann, G. C. A. M. Janssen, S. E. Zhu, P. Jarillo-Herrero, M. M. Fogler, D. N. Basov, *Nat. Nanotechnol.* **2015**, *10*, 682.
[39] Y. Fan, X. He, F. Zhang, W. Cai, C. Li, Q. Fu, N. V. Sydorchuk, S. L. Prosvirnin, *Research* **2021**, *2021*, 9754083.
[40] X. G. Luo, M. B. Pu, X. Li, X. L. Ma, *Light Sci. Appl.* **2017**, *6*, e16276.
[41] X. Liu, T. Starr, A. F. Starr, W. J. Padilla, *Phys. Rev. Lett.* **2010**, *104*, 207403.
[42] W. Zhu, Y. Fan, C. Li, R. Yang, S. Yan, Q. Fu, F. Zhang, C. Gu, J. Li, *Nanoscale* **2020**, *12*, 8758.
[43] I. Staude, A. E. Miroshnichenko, M. Decker, N. T. Fofang, S. Liu, E. Gonzales, J. Dominguez, T. S. Luk, D. N. Neshev, I. Brener, *ACS Nano* **2013**, *7*, 7824.
[44] A. B. Evlyukhin, S. M. Novikov, U. Zywietz, R. L. Eriksen, C. Reinhardt, S. I. Bozhevolnyi, B. N. Chichkov, *Nano Lett.* **2012**, *12*, 3749.
[45] Y. Zhou, W. Wu, R. Chen, W. Chen, R. Chen, Y. Ma, *Adv. Opt. Mater.* **2019**, *8*, 1901523.
[46] X. Ni, N. K. Emani, A. V. Kildishev, A. Boltasseva, V. M. Shalaev, *Science* **2012**, *335*, 427.
[47] N. Meinzer, W. L. Barnes, I. R. Hooper, *Nat. Photonics* **2014**, *8*, 889.
[48] A. Pors, M. G. Nielsen, R. L. Eriksen, S. I. Bozhevolnyi, *Nano Lett.* **2013**, *13*, 829.
[49] L. Liu, X. Zhang, M. Kenney, X. Su, N. Xu, C. Ouyang, Y. Shi, J. Han, W. Zhang, S. Zhang, *Adv. Mater.* **2014**, *26*, 5031.
[50] S. Sun, Q. He, S. Xiao, Q. Xu, X. Li, L. Zhou, *Nat. Mater.* **2012**, *11*, 426.
[51] C. Pfeiffer, A. Grbic, *Phys. Rev. Lett.* **2013**, *110*, 197401.
[52] M. Decker, I. Staude, M. Falkner, J. Dominguez, D. N. Neshev, I. Brener, T. Pertsch, Y. S. Kivshar, *Adv. Opt. Mater.* **2015**, *3*, 813.
[53] M. Khorasaninejad, W. T. Chen, R. C. Devlin, J. Oh, A. Y. Zhu, F. Capasso, *Science* **2016**, *352*, 1190.
[54] S.-C. Jiang, X. Xiong, Y.-S. Hu, S.-W. Jiang, Y.-H. Hu, D.-H. Xu, R.-W. Peng, M. Wang, *Phys. Rev. B* **2015**, *91*, 125421.
[55] K. E. Chong, I. Staude, A. James, J. Dominguez, S. Liu, S. Campione, G. S. Subramania, T. S. Luk, M. Decker, D. N. Neshev, *Nano Lett.* **2015**, *15*, 5369.
[56] Y. F. Yu, A. Y. Zhu, R. Paniagua-Domínguez, Y. H. Fu, B. Luk'yanchuk, A. I. Kuznetsov, *Laser Photonics Rev.* **2015**, *9*, 412.
[57] K. E. Chong, L. Wang, I. Staude, A. R. James, J. Dominguez, S. Liu, G. S. Subramania, M. Decker, D. N. Neshev, I. Brener, *ACS Photonics* **2016**, *3*, 514.
[58] W. Liu, Z. Li, Z. Li, H. Cheng, C. Tang, J. Li, S. Chen, J. Tian, *Adv. Mater.* **2019**, *31*, 1901729.
[59] L. Li, J. Zhang, Y. Hu, J. Lai, S. Wang, P. Yang, X. Li, H. Duan, *Laser Photonics Rev.* **2021**, *15*, 2100198.
[60] Z. L. Deng, Q. A. Tu, Y. Wang, Z. Q. Wang, T. Shi, Z. Feng, X. C. Qiao, G. P. Wang, S. Xiao, X. Li, *Adv. Mater.* **2021**, *33*, 2103472.
[61] Q. Song, A. Baroni, P. C. Wu, S. Chenot, V. Brandli, S. Vézian, B. Damilano, P. de Mierry, S. Khadir, P. Ferrand, *Nat. Commun.* **2021**, *12*, 3631.
[62] A. Arbabi, Y. Horie, M. Bagheri, A. Faraon, *Nat. Nanotechnol.* **2015**, *10*, 937.
[63] N. Yu, P. Genevet, M. A. Kats, F. Aieta, J.-P. Tetienne, F. Capasso, Z. Gaburro, *Science* **2011**, *334*, 333.
[64] A. Díaz-Rubio, V. S. Asadchy, A. Elsakka, S. A. Tretyakov, *Sci. Adv.* **2017**, *3*, e1602714.